Variable Rate Adaptive Modulation for DS-CDMA

Vincent K. N. Lau and Svetislav V. Maric

***Abstract*— An adaptive coding scheme is introduced for a discrete sequence code-division multiple-access system. The system uses noncoherent M-ary orthogonal modulation with RAKE receiver and power control. Both a fast fading channel and a combined fast fading, shadowing and power control channel are considered. Analytical bounds and simulations are done to evaluate the performance of the system. It is found that there are significant improvement in the average throughput and the bit-error-rate performance in the adaptive coding scheme. The amount of improvement drops with the increase of diversity branches used. More importantly, it is found that adaptive coding scheme is relatively robust to shadowing, while fix-rate codes are ineffective in the shadowing environment. Finally, adaptive coding scheme is found to be robust to mobile speed, feedback delay, and finite interleaving depth.**

***Index Terms*— Adaptive coding, code-division multiple-access, modulation.**

I. Introduction

TRADITIONAL fix-rate error correction code (ECC) failed to exploit the time-varying nature of the mobile radio channels. The channel is good most of the time and only occasionally under deep fade. Fix-rate ECC is designed for the average or the worst-case situation. On the other hand, variable rate adaptive channel coding (VRAECC) can adapt to the changing channel conditions. During good channel conditions, more information can be sent with less error protection but when the channel conditions become worse, we use more powerful code for more protection. In [1]–[5], it was shown that VRAECC increases the average throughput compared with traditional fix-rate codes.

In this paper, we propose, for the first time, a variable rate adaptive ECC (VRAECC) system for high bandwidth-expansion systems such as discrete sequence code-division multiple-access system (DS-CDMA). Note that inherited differences between time-division multiple-access (TDMA) systems [1], [6], and DS-CDMA systems warrant a completely different design and analysis of the VRAECC. For instance, frequency selective fading channel model with power delay profile is used in the analysis [7]. In CDMA, RAKE receiver is often used to provide frequency diversity. The fading statistics will be different and a reduction in the performance gain of the VRAECC scheme will be expected.[1]

In the analysis, we assume the system experiences Rayleigh fading, as well as log-normal shadowing. M-ary orthogonal modulation and noncoherent detection are used. Performance analysis of M-ary orthogonal modulation CDMA system with RAKE receiver has appeared in many papers such as [8], [9]. However, none of them, has considered coding combined with M-ary noncoherent orthogonal modulation, RAKE receiver, power delay profile and shadowing together. Furthermore, the approximation method introduced in [8] cannot be applied here due to variable system throughput. Due to the complexity involved in deriving an analytical bound in noncoherent detection and variable throughput system, zero-feedback delay, and ideal interleaving are assumed in the analysis. The robustness of the VRAECC scheme w.r.t. finite interleaving depths, feedback delays, and mobile speeds are investigated by simulations.

The paper is organized as follows. In Section II, the design and the operation of the VRAECC scheme are discussed. The channel models for fast fading and shadowing are discussed in Section III. The performance analysis of VRAECC scheme under noncoherent, RAKE and fast fading only, as well as under combined fast fading and shadowing are discussed in Section IV. Simulation method is described in Section V. Results from theories and simulations are presented and discussed in Section VI. Finally, we conclude with a brief summary of results in Section VII.

II. Variable Rate Noncoherent Orthogonal Modulation (VRNOM)

In this section, we shall discuss design and operation of the proposed VRNOM. The following list the important design criteria.

1) *Rate Compatibility and Minimum Distance Preserving:* It is desirable to have a class of completely rate compatible[2] or minimum distance preserving codes.
2) *Constant Bandwidth:* It is desirable to have a constant occupied bandwidth as the throughput changes.
3) *Single Decoder:* It is desirable to use a class of variable rate ECC's that have a common basic structure so that a single decoder can be used.

A. System Description of the VRNOM

Fig. 1 shows a simplified block diagram of the VRNOM system.

Paper approved by B. D. Woerner, Editor for Wireless Spread Spectrum of the IEEE Communications Society. Manuscript received June 26, 1996; revised August 15, 1997. This work was presented in part at the ICPMSC'96 (2nd International Conference on Personal Mobile and SS Communications), Hong Kong, December 1996.

V. K. N. Lau is with the Department of Electrical and Electronic Engineering, University of Hong Kong, Pokulam, Hong Kong (e-mail: knlau@eee.hku.hk).

S. V. Maric is with Qualcomm Inc., San Diego, CA 92121 USA (e-mail: smaric@qualcomm.com).

Publisher Item Identifier S 0090-6778(99)02168-6.

[1] As the order of diversity increases, the variance of the signal strength (in decibels) will be reduced [7].

[2] Complete rate compatibility means that the Hamming distance of an error path is not reduced as a result of throughput transition from a lower rate to a higher rate or vice versa.

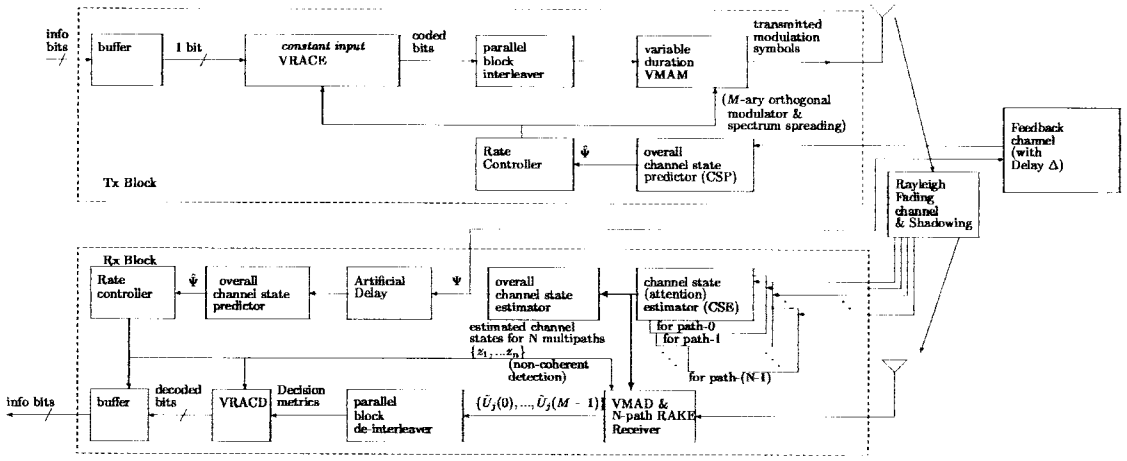

Fig. 1. Simplified block diagram of VRNOM system.

The transmitter consists of a *constant input* variable rate adaptive channel encoder (VRACE), a variable constellation (as well as variable duration) modulator, a parallel block interleaver, a channel state predictor (CSP), and a rate controller. The receiver consists of a corresponding variable rate channel decoder, a variable constellation demodulator which is a square law detector and a RAKE receiver. Information bits are buffered. Noncoherent detection is used which eliminates the need for channel phase estimation at the receiver. Current channel state is predicted by the CSP at transmitter based on the past feedback channel states. Appropriate throughput mode is used based on the predicted state. Tx–Rx synchronization is achieved by *quasi-closed loop* control mechanism (see Section II-D). Mode-3 is chosen to be the reference code for comparison. Some important system components are described below.

1) Design of VRACE: A *constant input* VRACE with $k = 1$ is used which consists of a class of convolution codes as illustrated in Fig. 2(a).

Code rates varying from $1/2$ to $1/9$ are achievable. Generator[3] given by $(1, 2, 4, 10)_8$ is used for rate-$1/4$ code. Generators of rate-$1/3$ and rate-$1/2$ codes are given by $(13, 15, 17)_8$ and $(15, 17)_8$, respectively. Rate-$1/5$ code is generated by $(1, 2, 4, 10, X)_8$ and so on where X means don't care. In the trellis diagram, there are altogether $2^4 = 16$ branches between each transition. Hence, within the range of rate-$1/4$ and rate-$1/9$, the VRACE achieves *complete rate-compatibility* since completely distinct labels (by the output bits) can be found for each branch. Complete rate-compatibility cannot be extended into rate-$1/3$ and rate-$1/2$ since there are not enough distinct branch labels. Nevertheless, *minimum-distance preserving* can be maintained across the full range of code rates.

2) Design of Modulator: A M-ary time orthogonal modulator is used. The VMAM takes $\log_2 M$ bits from the VRACE and transform them into M orthogonal bits, $\{v_{m,l} = \pm 1\}$, $l \in [0, M-1]$, by Walsh–Hadamard mapping [10] where each modulation symbol[4] (or orthogonal code sequence) is labeled by m with $m \in [0, M-1]$. Spectrum spreading is achieved by feeding M orthogonal bits into an I-Q modulator where they are mixed with two short and independent pseudorandom sequences (PN).[5] This is illustrated in Fig. 2(b). Hence an M-ary orthogonal modulation symbol consists of M basic symbols. Variable modulation throughput is achieved by varying M. Since the basic symbol has constant duration, physical bandwidth is kept constant. Note that both the modulation symbol duration and the constellation level (dimensionality) are varying as the modulation throughput. The VMAM is matched with the VRACE by mapping one M-ary modulation symbol per trellis transition. Overall system throughput from $1/2^2$ to $1/2^9$ can be achieved by combining the VMAM and the VRACE. Hence, there are eight throughput modes listed as follows. We label each modes as follows:

- *Mode 0: Rate* $1/9$ code + 2^9-ary orthogonal modulator;
- *Mode 1: Rate* $1/8$ code + 2^8-ary orthogonal modulator;
- ...
- *Mode 7: Rate* $1/2$ code + 2^2-ary orthogonal modulator.

3) Design of Interleaver: The channel state memory is eliminated by means of interleaving. However, due to the variable modulation symbol duration, the interleaving task is not trivial. The interleaver has no way of knowing the channel states for each input symbol before they are actually transmitted. Fig. 2(c) shows a possible implementation of the interleaver, namely *parallel interleaving*, for the VRNOM scheme. For each information bit, different number of coded bits corresponding to the eight throughput modes are fed into eight block interleavers in parallel. Along each branch, encoding and interleaving occur as if it were a fix-rate coding scheme. All the outputs of the interleavers from the branches are fed into a selector in VMAM which selects a channel symbol from one of the branches depending on the rate control signal. In this way, interleaving can be implemented.

4) Design of Demodulator: The simplified decoder structure is shown in Fig. 2(d). The decoder consists of N or-

[3]Constraint length of 4 is used.

[4]The label of each modulation symbol, m, is the binary equivalent of the $\log_2 M$ bits.

[5]In IS-95, M-ary symbols are first randomized by a long period PN sequence which is unique for each user. The I, Q PN's are the same within each cell. For simplicity, we assume that only the short I, Q random sequences are used.

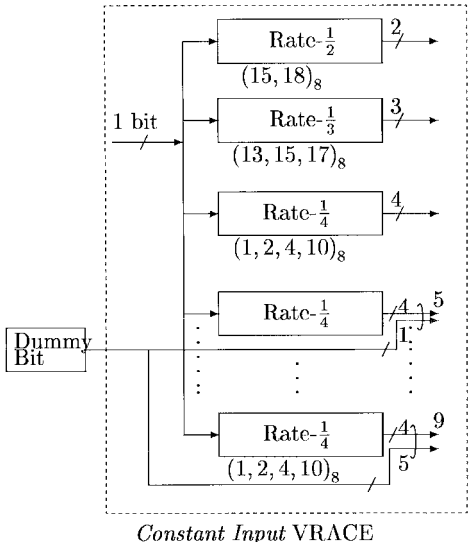

(a)

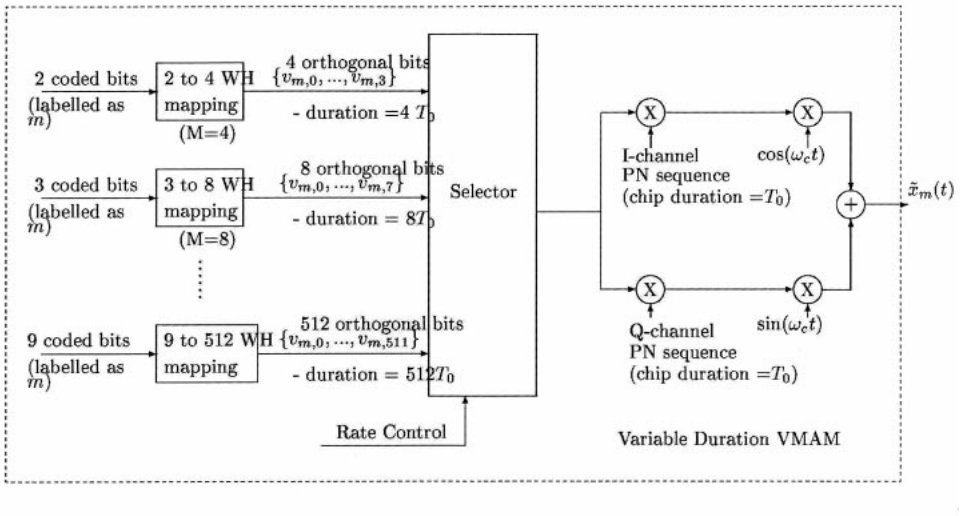

(b)

Fig. 2. System components of VRNOM.

thogonal demodulators (square-law detectors) for N resolvable multipaths. Since a modulation symbol is an M-dimensional signal, the nth detector gives a set of M branch decision metrics, $\{U_n(0), \cdots, U_n(M-1)\}$ for every received symbol. The N branch metric sets are then combined to give a set of final branch decision metrics, $\{\tilde{U}(0), \cdots, \tilde{U}(M-1)\}$ which are used in the Viterbi decoder for soft decision decoding.

Since the VRACE trellis has a time-invariant basic structure, a common Viterbi decoder can be used to decode all the codes. The square-law detector in VMAD has to adjust its correlation duration (which is in integral step) for different throughput modes to supply the appropriate branch metric. This greatly simplifies the decoder design for adaptive demodulation.

B. Transfer Functions of the VRACE

Since one M-ary modulation symbol corresponds to a single trellis transition, the system can be analyzed in GF(M). The weight enumerating functions of mode-0 to mode-5 codes are given by (see [20])

$$\left.\frac{\partial T(P,W)}{\partial P}\right|_{P=1} = W^4 + 2W^5 + 5W^6 + 8W^7 + \cdots. \quad (1)$$

The weight enumerating functions for the mode-6 and mode-7 codes are given by $W^4 + 2W^5 + 6W^6 + 8W^7 + \cdots$ and $2W^4 + 8W^5 + 11W^6 + 2W^7 + \cdots$, respectively.

C. Operation of the Adaptive Code

The predicted overall-channel-state, $\hat{\Psi}$, is partitioned into eight segments with each segment corresponding to one of the throughput modes. Let $E_s/(\eta_0 + I_0)$ be the average reference symbol-energy-to-noise-plus-interference ratio (SIR). The predicted instantaneous-SIR, $\hat{\gamma}$, is given by

$$\hat{\gamma} = \left|\hat{\Psi}\right|^2 \frac{E_s}{\eta_0 + I_0}. \quad (2)$$

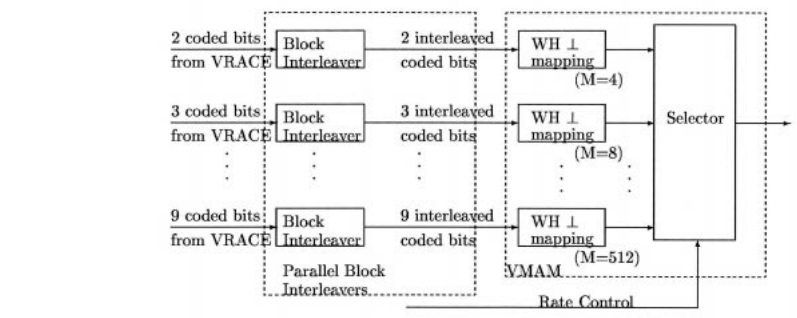

(a)

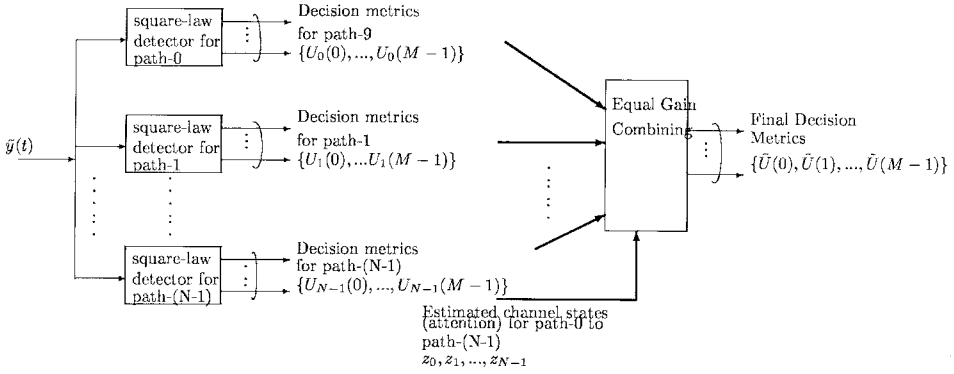

(b)

Fig. 3. System components of VRNOM.

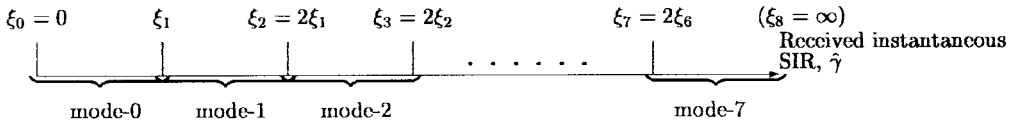

Fig. 4. Illustration of adaptation thresholds on predicted.

Mode-q is chosen if $\hat{\gamma} \in [\zeta_q, \zeta_{q+1}]$ where $\{\zeta_0, \zeta_1, \cdots, \zeta_8\}$ are control parameters called the *adaptation thresholds*. Note that $\zeta_0 = 0$ and $\zeta_8 = \infty$. We choose the thresholds in 3 dB steps as illustrated in Fig. 4. Hence, the overall performance is controlled by a single parameter, ζ_1, only. Two operations, namely *constant bit-error rate (BER)* and *constant throughput*, are possible. For the *constant BER* operation, ζ_1 is constant. For the *constant throughput* operation, $\zeta_1 \propto \hat{\gamma}$.

D. Tx–Rx Synchronization

The channel state predictor (CSP) at the transmitter predicts the current channel state based on the feedback channel state information from the receiver with a certain delay. Modulation modes for individual symbols are based on the predicted channel states. The receiver has perfect knowledge of the channel states at the input of the transmitter CSP. By using the same CSP at the receiver and feeding in a delay compensated stream of channel states, the same modulation mode sequence can be generated at the receiver. Hence, the Tx–Rx synchronization can be maintained by synchronizing the feedback delay. This can be done easily by periodically reporting the feedback delay from the transmitter to the receiver.

III. Fading Statistics

The system consists of a single cell with K mobile users. All users are equipped with VRNOM modem and they operate independently based on individual signal strength measurements.

A. Multipath Fading

We assume fading is slow enough so that channel attenuations are highly correlated within one M-ary symbol duration. Hence, orthogonality between different M-ary symbols is maintained.[6]

The received instantaneous SIR for the nth path, γ_n, and the total received instantaneous SIR, γ, are given by

$$\gamma_n = c_n^2 \frac{E_s}{\eta_0 + I_0} \tag{3}$$

[6]This is a realistic assumption since for an average reference symbol rate of 40 kB, the average reference modulation symbol duration is 0.025 ms. The coherence time for the mobile channel is in the range of 30 to 1 ms for the mobile speed of 2.5 to 75 km/h. Hence, fading will be constant within at least one symbol duration for all throughput modes.

and

$$\gamma = \sum_{n=0}^{N-1} c_n^2 \frac{E_s}{\eta_0 + I_0}. \tag{4}$$

γ_n is exponentially distributed with density function given by

$$f_{\gamma_n|\overline{\gamma}_n}(\gamma_n) = \frac{1}{\overline{\gamma}_n} e^{-(\gamma_n/\overline{\gamma}_n)} \tag{5}$$

where $\overline{\gamma}_n$ is the local mean of γ_n. Since channel fading for the N multipaths is independent, the distribution of γ is the N-*fold* convolution of (5), given by

$$f_{\gamma|\overline{\gamma}}(\gamma) = \sum_{n=0}^{N-1} \frac{\pi_n}{\overline{\gamma}_n} e^{-(\gamma/\overline{\gamma}_n)} \tag{6}$$

where

$$\pi_n = \prod_{\substack{i=0 \\ i\neq n}}^{N-1} \frac{\overline{\gamma}_n}{\overline{\gamma}_n - \overline{\gamma}_i}. \tag{7}$$

In order to use (6) in BER calculation in Section IV, we need to express the RHS of (6) in terms of the local mean, $\overline{\gamma}$. Assume that the power delay profile[7] of the channel is given by

$$P_h(\tau) = A_0 e^{-\tau B_c} \tag{8}$$

where A_0 is a constant. Further assume that $P_h(nT_c + \delta) \approx P_h(nT_c) = A_0 e^{-(n/\epsilon)}$ for $|\delta| < T_c/2$ where $\epsilon = 1/T_c B_c \approx N - \frac{1}{2}$. The local mean, $\overline{\gamma}_n$ and $\overline{\gamma}$, are given by

$$\overline{\gamma}_n \propto P_h(nT_c) \qquad \overline{\gamma} = \sum_{n=0}^{N-1} \overline{\gamma}_n \propto \frac{1 - e^{-(N/\epsilon)}}{1 - e^{-(1/\epsilon)}}.$$

Express $\overline{\gamma}_n$ in terms of the local mean, $\overline{\gamma}$, we have:

$$\overline{\gamma}_n = \overline{\gamma} A_1 e^{-(n/\epsilon)} \tag{9}$$

where

$$A_1 \stackrel{\text{def}}{=} \left[\frac{1 - e^{-(1/\epsilon)}}{1 - e^{-(N/\epsilon)}}\right].$$

Hence, substituting (9) into (7), the distribution of the total received instantaneous SIR, γ, in terms of the local mean, $\overline{\gamma}$, is given by

$$f_{\gamma|\overline{\gamma}}(\gamma) = \sum_{n=0}^{N-1} \frac{\pi_n}{\overline{\gamma} A_1 e^{-(n/\epsilon)}} \exp\left(-\frac{p}{\overline{\gamma} A_1 e^{-(n/\epsilon)}}\right) \tag{10}$$

with

$$\pi_n = \prod_{\substack{i=0 \\ i\neq n}}^{N-1} \frac{e^{-(n/\epsilon)}}{e^{-(n/\epsilon)} - e^{-(i/\epsilon)}}.$$

[7]The power delay profile gives the average power received from paths with delay τ, i.e., $\frac{1}{2}E[\bar{h}^*(\tau_1)h(\tau_2)] = P_h(\tau_1)\delta(\tau_1 - \tau 2)$ where $\bar{h}(\tau)$ is the channel impulse response.

B. Shadowing and Power Control

Shadowing in mobile radio channels is usually modeled as log-normal distribution with variance of the local mean, $\overline{\gamma}$, ranges from 6 to 9 dB. It is a slow process so that a block of symbols is shadowed by the same amount and this correlated shadowing cannot be removed by interleaving. Power control is used to combat log-normal fading and path loss. It equalizes the received signal strengths of all users on the reverse link. However, because of delay in executing power control commands, shadowing cannot be completely removed, causing received signal power fluctuations as mobiles move in the cell. It is shown in a field test that signal fluctuations after imperfect power control can be fitted accurately by a log-normal distribution with the variation ranging from 2.8 to 4.5 dB [11].

We assume the variance of local mean in decibels, $\sigma^2_{\overline{\gamma}_{\text{dB}}}$, to be 3 dB. Hence, the distribution of the local mean is given by

$$f_{\overline{\gamma}}(\overline{\gamma}) = \frac{A_2}{\sqrt{2\pi}\,\sigma_{\overline{\gamma}_{\text{dB}}}\overline{\gamma}} e^{-\left(1/2\sigma^2_{\overline{\gamma}_{\text{dB}}}\right)\left(\overline{\gamma}_{\text{dB}} - \mu_{\overline{\gamma}_{\text{dB}}}\right)^2} \tag{11}$$

where $\overline{\gamma}_{\text{dB}} = 10\log_{10}(\overline{\gamma})$ and $A_2 = 10/\log_e(10)$.

IV. Rake Receiver and Error Analysis

In this section, we derive an analytical expressions for the error performance of the proposed VRNOM system. The analysis is based on the reverse link of DS-CDMA systems where it is more capacity limiting. Because it is not feasible to maintain phase synchronization in the reverse link, noncoherent detection is used. To benefit from the wide-band CDMA signal, N-paths RAKE receiver is used to provide frequency diversity. Error performance in Rayleigh fading channel as well as channel combined with Rayleigh fading and shadowing are analyzed. Due to huge complexity involved in deriving error bounds in noncoherent detection, ideal situations are assumed. Two important assumptions are listed below:

i) ideal interleaving.
ii) zero feedback delay and ideal channel state prediction at the transmitter.

The effects of these assumptions on actual performance are investigated by simulations.

A. RAKE Receiver Processing

Let index (i) denotes the ith user, E_0 be the chip energy or basic symbol energy, T_0 be the chip duration, $m^{(i)}$ denotes the transmitted modulation symbol, $a_l^{(i)}(I) = \{\pm 1\}$ and $a_l^{(i)}(Q) = \{\pm 1\}$ be the I and Q PN sequence, the transmitted signal for the ith user, $\tilde{x}^{(i)}_{m^{(i)}}(t)$, is given by (in low-pass equivalent)

$$\tilde{x}^{(i)}_{m^{(i)}}(t) = \sqrt{\frac{E_0}{T_0}}\, v\Big(m^{(i)}, t\Big)\tilde{a}^{(i)}(t) \tag{12}$$

where

$$v\left(m^{(i)}, t\right) = \sum_{l=0}^{M-1} v_{m^{(i)},l} p(t - lT_0), \quad t \in \left[0, T_s\left(q^{(i)}\right)\right]$$

$$\tilde{a}^{(i)}(t) = a_I^{(i)}(t) + j a_Q^{(i)}(t)$$

$$a_I^{(i)}(t) = \sum_{l=0}^{M-1} a_l^{(i)}(I) p(t - lT_0)$$

$$a_Q^{(i)}(t) = \sum_{l=0}^{M-1} a_l^{(i)}(Q) p(t - lT_0)$$

$p(t)$ is the transmitted pulse shape of duration T_0 (rectangular pulse is assumed), and $T_s(q^{(i)})$ is the modulation symbol duration of user-i transmitting at mode-$q^{(i)}$.

Assume that user-k suffers a delay of $\tau^{(k)}$ and that, WLOG, let $\tau^{(i)} = 0$. Because of the wide-band signal used in DS-CDMA, frequency selective fading is experienced by the signal. The channel impulse response is given by

$$\tilde{h}(t) = \sum_{n=0}^{N-1} c_n e^{-j\phi_n} \delta(t - nT_0). \tag{13}$$

The received signal for the ith user, $\tilde{y}^{(i)}(t)$, is given by

$$\begin{aligned}\tilde{y}^{(i)}(t) &= \int_0^\infty \tilde{h}(\tau)\tilde{x}(t-\tau)\,d\tau + \tilde{n}(t) \\ &= \sum_{n=0}^{N-1} c_n^{(i)} e^{-j\phi_n^{(i)}} \tilde{x}_{m^{(i)}}^{(i)}(t - nT_0) \\ &\quad + \sum_{\substack{k=1 \\ k\neq i}}^{K} \sum_{n=0}^{N-1} c_n^{(k)} e^{-j\left(\omega_c \tau^{(k)} + \phi_n^{(k)}\right)} \tilde{x}_{m^{(k)}}^{(k)} \\ &\quad \cdot \left(t - nT_0 - \tau^{(k)}\right) + \tilde{n}(t)\end{aligned}$$

where $\tilde{n}(t)$ denotes the white Gaussian channel noise, index-n denotes the nth path in the fading channel and index-(k) denotes the signal corresponding to the kth user.

As described in Section II-A-4, since the channel phase $\phi_n^{(i)}$ is unknown, equal gain combining is used in the RAKE receiver to combine the branch metrics from individual path. Let $\hat{m}^{(i)}$ be the estimated modulation symbol for user-i. Consider the nth path receiver and neglect the intersymbol interference,[8] the decision metric for the nth path of the ith user is shown in (13a), shown at the bottom of the page, where

$$\rho_{m^{(i)}, \hat{m}^{(i)}}^{(i,i)}(\tau) \stackrel{\text{def}}{=} \frac{1}{\sqrt{E_s\left(q^{(i)}\right)}} \int_0^{T_s\left(q^{(i)}\right)} \tilde{x}_{m^{(i)}}^{(i)}(t) \tilde{x}_{\hat{m}^{(i)}}^{*(i)}(t-\tau)\,dt \tag{14}$$

$$\rho_{m_k, \hat{m}^{(i)}}^{(k,i)}(\tau) \stackrel{\text{def}}{=} \frac{1}{\sqrt{E_s\left(q^{(i)}\right)}} \int_0^{T_s\left(q^{(i)}\right)} \tilde{x}_{m_k}^{(k)}(t) \tilde{x}_{\hat{m}^{(i)}}^{*(i)}(t-\tau)\,dt \tag{15}$$

and

$$\begin{aligned}N_n^{(i)} &\stackrel{\text{def}}{=} \frac{1}{\sqrt{E_s\left(q^{(i)}\right)}} \int_0^{T_s\left(q^{(i)}\right)} \tilde{n}(t) \tilde{x}_{\hat{m}^{(i)}}^{*}(t)\,dt \\ &\stackrel{\text{def}}{=} N_n^{(i)}(\Re) + j N_n^{(i)}(\Im).\end{aligned} \tag{16}$$

Express the decision metric for the nth detector, $U_n^{(i)}(\hat{m}^{(i)})$, as

$$U_n^{(i)}(\hat{m}^{(i)}) \stackrel{\text{def}}{=} \left[U_n^{(i)}(\hat{m}, \Re)\right]^2 + \left[U_n^{(i)}(\hat{m}, \Im)\right]^2. \tag{17}$$

.

For DS-CDMA, the self interference and the multiple access interference (MAI) at the front end of the receiver can be modeled as additive white Guassian noise. For multipath

[8]It is shown in [12] that the intersymbol interference of the RAKE receiver is negligible when the symbol duration is long enough. In our case, $T_s(0) = 512T_0$ and $T_s(7) = 4T_0$. These justify the assumption.

$$\begin{aligned}U_n^{(i)}\left(\hat{m}^{(i)}\right) &= \left| \frac{1}{\sqrt{E_s\left(q^{(i)}\right)}} \int_{nT_0}^{nT_0 + T_s\left(q^{(i)}\right)} \tilde{y}(t) \tilde{x}_{\hat{m}^{(i)}}^{*(i)}(t - nT_0)\,dt \right|^2 \\ &= \Bigg| \underbrace{c_n^{(i)} e^{-j\phi_n^{(i)}} \rho_{m^{(i)}, \hat{m}^{(i)}}^{(i,i)}(0)}_{\text{signal term}} + \underbrace{\sum_{\substack{n'=0 \\ n'\neq n}}^{N-1} c_{n'}^{(i)} e^{-j\phi_{n'}^{(i)}} \rho_{m^{(i)}, \hat{m}^{(i)}}^{(i,i)}((n-n')T_0)}_{\text{self interference}} \\ &\quad + \underbrace{\sum_{n'=0}^{N-1} \sum_{\substack{k=1 \\ k\neq i}}^{K} c_{n'}^{(k)} e^{-j\left(\phi_{n'}^{(k)} + \omega_c \tau^{(k)}\right)} \rho_{m^{(k)}, \hat{m}^{(i)}}^{(k,i)}\left((n-n')T_0 - \tau^{(k)}\right)}_{\text{Multiple Access Int. (MAI)}} + \underbrace{N_n^{(i)}}_{\text{Channel Noise}} \Bigg|^2\end{aligned} \tag{13a}$$

fading channels, a rigorous comparison of a Guassian approximation with more accurate approximations has been made [13], [14]. These results show that the Guassian approximation is sufficiently accurate even for small K and large signal power. The self interference and MAI are analyzed below.

1) Self Interference: The mean of the self interferences, $U_n^{(i)}\left(\hat{m}^{(i)}, \Re, i, i\right)$ and $U_n^{(i)}\left(\hat{m}^{(i)}, \Im, i, i\right)$, are easily shown to be zero. The variances are given by [15]

$$\sigma^2_{U_n^{(i)}\left(\hat{m}^{(i)}, \Re, i, i\right)} = \frac{4E_s}{3\text{PG(ref)}} \sum_{\substack{n'=0 \\ n' \neq n}}^{N-1} \mathcal{E}\left[\left(c_{n'}^{(i)}\right)^2\right] \tag{18}$$

$$\sigma^2_{U_n^{(i)}\left(\hat{m}^{(i)}, \Im, i, i\right)} = \frac{4E_s}{3\text{PG(ref)}} \sum_{\substack{n'=0 \\ n' \neq n}}^{N-1} \mathcal{E}\left[\left(c_{n'}^{(i)}\right)^2\right] \tag{19}$$

where PG(ref) is the reference processing gain given by T_s/T_0 and E_s is the reference modulation symbol energy.

2) Multiple Access Interference: The means of the MAI's, $U_n^{(i)}\left(\hat{m}^{(i)}, \Re, k, i\right)$ and $U_n^{(i)}\left(\hat{m}^{(i)}, \Im, k, i\right)$, are easily shown to be zero. The variances are given by [15]

$$\sigma^2_{U_n^{(i)}\left(\hat{m}^{(i)}, \Re, k, i\right)} = \frac{4E_s}{3\text{PG(ref)}} \sum_{\substack{k=1 \\ k \neq i}}^{K} \sum_{n'=0}^{N-1} \mathcal{E}\left[\left(c_{n'}^{(k)}\right)^2\right] \tag{20}$$

$$\sigma^2_{U_n^{(i)}\left(\hat{m}^{(i)}, \Im, k, i\right)} = \frac{4E_s}{3\text{PG(ref)}} \sum_{\substack{k=0 \\ k \neq i}}^{K} \sum_{n'=0}^{N-1} \mathcal{E}\left[\left(c_{n'}^{(k)}\right)^2\right]. \tag{21}$$

3) Channel Noise: The variances of the channel noise terms are given by

$$\sigma^2_{N_n^{(i)}(\Re)} = \sigma^2_{N_n^{(i)}(\Im)} = 2\eta_0. \tag{22}$$

4) Decision Metric: Assume the self interference, MAI, and the channel noise terms are mutually independent zero mean Guassian random variables. The *total noise,*[9] denoted by $\Upsilon_n^{(i)}(\Re)$ and $\Upsilon_n^{(i)}(\Im)$ is given by

$$\Upsilon_n^{(i)}(\Re) \stackrel{\text{def}}{=} N_n^{(i)}(\Re) + U_n^{(i)}\left(\hat{m}^{(i)}, \Re, i, i\right) + U_n^{(i)}(\hat{m}, \Re, k, i)$$
$$\Upsilon_n^{(i)}(\Im) \stackrel{\text{def}}{=} N_n^{(i)}(\Im) + U_n^{(i)}\left(\hat{m}^{(i)}, \Im, i, i\right) + U_n^{(i)}\left(\hat{m}^{(i)}, \Im, k, i\right).$$

The variances of $\Upsilon_n^{(i)}(\Re)$ and $\Upsilon_n^{(i)}(\Im)$ are both equal and denoted by $(\sigma_{\Upsilon_n}^{(i)})^2$. From (18) to (22), we have[10] the variance of the total noise written as

$$\left(\sigma_{\Upsilon_n}^{(i)}\right)^2 = 4\left[\frac{\eta_0}{2} + \frac{E_s}{3\text{PG(ref)}} \sum_{k=1}^{K} \sum_{n'=0}^{N-1} \mathcal{E}\left[\left(c_{n'}^{(k)}\right)^2\right]\right].$$

Because the fading attenuations $(c_n^{(k)})^2$ is independent of k and we can drop the superscript k. The variance is then denoted by σ_Υ^2 and is written as

$$\sigma_\Upsilon^2 = 4\left[\frac{\eta_0}{2} + \frac{KE_s}{3\text{PG(ref)}} \sum_{n'=0}^{N-1} \mathcal{E}\left[(c_{n'})^2\right]\right]. \tag{23}$$

The decision metric for the nth receiver of the ith user is thus given by (24) and (25), shown at the bottom of the page.

After equal gain combining of all the N detectors' output, the combined decision metrics are given by

$$\tilde{U}^{(i)}\left(\hat{m}^{(i)}\right) = \sum_{n=0}^{N-1} \left\{\left[U_n^{(i)}\left(\hat{m}^{(i)}, \Re\right)\right]^2 \left[U_n^{(i)}\left(\hat{m}^{(i)}, \Im\right)\right]^2\right\}. \tag{26}$$

B. Viterbi Decoding and Decision Statistics

Decision metrics $\{\tilde{U}^{(i)}(\hat{m}^{(i)})\}$ for each received symbol obtained in the previous section are fed into a Viterbi decoder to calculate path decision metrics. Let index j denotes the jth trellis transition. Assume that all zero bit sequence is transmitted ($m_j^{(i)} = 0$). Estimated path, labeled as p_1, separates from the transmitted path at node-0 and remerged with it at node-B_{p_1}. D denote the error path Hamming distance of the codes in GF(M). Adding subscript j into (26), the branch metric for the estimated path at the jth trellis transition is given by

$$\tilde{U}_j^{(i)}\left(\hat{m}_j^{(i)}\right) = \sum_{n=0}^{N-1} \left\{\left[U_{n,j}^{(i)}\left(\hat{m}_j^{(i)}, \Re\right)\right]^2 + \left[U_{n,j}^{(i)}\left(\hat{m}_j^{(i)}, \Im\right)\right]^2\right\}$$
$$\cdot \hat{m}_j^{(i)} \in [0, M-1] \tag{27}$$

where $\{\hat{m}_1^{(i)}, \hat{m}_2^{(i)}, \cdots, \hat{m}_{B_p}^{(i)}\}$ denotes the estimated symbol sequence along the p_1 path. Hence, the path metrics for the transmitted path, $CM^{(i)}(0)$, and the estimated path, $CM^{(i)}(p_1)$, in the code trellis are given by

$$CM^{(i)}(0) = \sum_{j=1}^{B_{p_1}} \sum_{n=0}^{N-1} \left\{\left[U_{n,j}^{(i)}(0, \Re)\right]^2 + \left[U_{n,j}^{(i)}(0, \Im)\right]^2\right\}$$

and

$$CM^{(i)}(p_1) = \sum_{j=1}^{B_{p_1}} \sum_{n=0}^{N-1} \left\{\left[U_{n,j}^{(i)}\left(\hat{m}_j^{(i)}, \Re\right)\right]^2 + \left[U_{n,j}^{(i)}\left(\hat{m}_j^{(i)}, \Im\right)\right]^2\right\}.$$

[9] The total noise is independent of m.

[10] Assume that $(\sigma_{\Upsilon_n}^{(i)})^2 \gg (4E_s/3\text{PG(ref)})\ \mathcal{E}[(c_n^{(i)})^2]$.

$$U_n^{(i)}\left(\hat{m}^{(i)}, \Re\right) = \begin{cases} \Lambda_n^{(i)}(0, \Re) \stackrel{\text{def}}{=} 2\sqrt{E_s\left(q^{(i)}\right)}\, c_n^{(i)} \cos\phi_n^{(i)} + \Upsilon_n^{(i)}(\Re), & \hat{m}^{(i)} = m^{(i)} \\ \Lambda_n^{(i)}(1, \Re) \stackrel{\text{def}}{=} \Upsilon_n^{(i)}(\Re), & \hat{m}^{(i)} \neq m^{(i)} \end{cases} \tag{24}$$

$$U_n^{(i)}\left(\hat{m}^{(i)}, \Im\right) = \begin{cases} \Lambda_n^{(i)}(0, \Im) \stackrel{\text{def}}{=} 2\sqrt{E_s\left(q^{(i)}\right)}\, c_n^{(i)} \sin\phi_n^{(i)} + \Upsilon_n^{(i)}(\Im), & \hat{m}^{(i)} = m^{(i)} \\ \Lambda_n^{(i)}(1, \Im) \stackrel{\text{def}}{=} \Upsilon_n^{(i)}(\Im), & \hat{m}^{(i)} \neq m^{(i)} \end{cases} \tag{25}$$

Because of the orthogonality between different M-ary symbols, the branch metric can only take either $\Lambda_{n,j}^2(0,\Re)+\Lambda_{n,j}^2(0,\Im)$ or $\Lambda_{n,j}^2(1,\Re)+\Lambda_{n,j}^2(0,\Im)$. Introducing index j to (24) and (25), dropping indices i,k when there is no ambiguity and substituting from (27), the difference between two path metrics is given by

$$\begin{aligned}\Delta CM &\stackrel{\text{def}}{=} CM(0)-CM(p_1)\\ &=\sum_{j=1}^{D}\sum_{n=0}^{N-1}\left\{[\Lambda_{n,j}(0,\Re)]^2+[\Lambda_{n,j}(0,\Im)]^2\right\}\\ &\quad-\sum_{j=1}^{D}\sum_{n=0}^{N-1}\left\{[\Lambda_{n,j}(1,\Re)]^2+\Lambda_{n,j}(1,\Im)\right\}\\ &\stackrel{\text{def}}{=}\chi_0-\chi_1. \end{aligned}\tag{28}$$

By expressing $E_s(q_j)$ in terms of the reference symbol energy E_s, we have $E_s(q_j)=E_s\times\xi(q_j)$, where

$$\xi(q_j)=\frac{T_s(q_j)}{T_s(3)}.\tag{29}$$

Define the total reference symbol energy for the modulation symbol at the jth trellis transition $\lambda_j^{(i)}$ as

$$\lambda_j\stackrel{\text{def}}{=}E_s\sum_{n=0}^{N-1}[c_{n,j}]^2\tag{30}$$

we have $\lambda_j=\xi_jE_s\sum_{n=0}^{N-1}[c_{n,j}]^2$.

Conditioning on $\{\lambda_j\}$, $\{c_{n,j}\}$, and $\{\phi_{n,j}\}$, the random variables $\Lambda_{n,j}(0,\Re)$ and $\Lambda_{n,j}(0,\Im)$ are Guassian random variables with mean $2\sqrt{E_s\xi_j}c_{n,j}\cos\phi_{n,j}$, $2\sqrt{E_s\xi_j}c_{n,j}\sin\phi_{n,j}$, and variances σ_Υ^2, respectively. $\Lambda_{n,j}(1,\Re)$ and $U_{n,j}(1,\Im)$ are zero-mean Guassian random variables with the same variances, σ_Υ^2. Hence, χ_0 and χ_1 are chi-square distributed (noncentral) with $2DN$ degrees of freedom. The noncentral parameter κ^2 is given by

$$\begin{aligned}\kappa^2&=\sum_{n=0}^{N-1}\sum_{j=1}^{D}\left\{\mathcal{E}^2[\Lambda_{n,j}(0,\Re)]+\mathcal{E}^2[\Lambda_{n,j}(0,\Im)]\right\}\\ &=4\sum_{j=1}^{D}\xi_j\lambda_j.\end{aligned}\tag{31}$$

The conditional first error event probability of the convolutional codes, denoted by $P_e(D|\{\lambda_j\},\{c_{n,j}\},\{\phi_{n,j}\})$, is given by [16]

$$\begin{aligned}&P_e(D|\{\lambda_j\},\{c_{n,j}\},\{\phi_{n,j}\})\\ &\quad=\Pr[\Delta CM<0|\{\lambda_j\},\{c_{n,j}\},\{\phi_{n,j}\}]\\ &\quad=\frac{1}{2^{2DN-1}}\exp\left(-\frac{\kappa^2}{4\sigma_\Upsilon^2}\right)\sum_{r=0}^{DN-1}K_r\left(\frac{\kappa^2}{4\sigma_\Upsilon^2}\right)^r\end{aligned}\tag{32}$$

where

$$K_r=\frac{1}{r!}\sum_{m=0}^{DN-1}\binom{2DN-1}{m}$$

and

$$\frac{\kappa^2}{4\sigma_\Upsilon^2}=\sum_{j=1}^{D}\frac{\lambda_j\xi_j}{2\left[\eta_0+\dfrac{2K}{3\text{PG(ref)}}\mathcal{E}(\lambda)\right]}.$$

Recall that γ_j is the instantaneous SIR in the jth symbol duration given by

$$\gamma_j=\frac{\lambda_j}{\eta_0+\dfrac{2K}{3\text{PG(ref)}}\mathcal{E}(\lambda)}.\tag{33}$$

Define $\gamma_j'=\frac{1}{2}\gamma_j$ to simplify notation. Then

$$\frac{\kappa^2}{4\sigma_\Upsilon^2}=\sum_{j=1}^{D}\gamma_j'\xi_j'.$$

It is seen from above that $\kappa^2/4\sigma_\Upsilon^2$ depends on λ_j and hence, γ_j' only. Therefore, the conditional first event error probability can be written as

$$\begin{aligned}&P_e(D|\{\lambda_j\},\{c_{n,j}\},\{\phi_{n,j}\})\\ &\quad=P_e(D|\{\lambda_j\})\\ &\quad=P_e(D|\{\gamma_j'\})\\ &\quad=\frac{1}{2^{2DN-1}}\exp\left(-\sum_{j=1}^{D}\gamma_j'\xi_j\right)\sum_{r=0}^{DN-1}K_r\left[\sum_{j=1}^{D}\gamma_j'\xi_j\right]^r.\end{aligned}\tag{34}$$

C. Average BER

The conditional BER $P_b(\text{error}|\{\gamma_j'\})$ is given by

$$P_b(\text{error}|\{\gamma_j'\})\le\sum_{D=D_{\min}}^{\infty}\beta_DP_e(D|\{\gamma_j'\})\tag{35}$$

where β_D is the coefficient of W^D in the weight enumerating function of the codes (1). To evaluate the average BER, we first evaluate the average first-event error probability, $P_e(D|\{\gamma_j'\})$. Two cases are considered in this section, namely Rayleigh fading only and combined Rayleigh fading and log-normal shadowing.

1) Rayleigh Fading Only: We concentrate on the variable rate scheme here. Any fix-rate scheme is a special case of VRNOM with a constant ξ_j. For Rayleigh fading channel, the variation of local mean is ignored. Hence, in the following derivation, we drop the local mean notation, $\overline{\gamma}$, in the conditioning variables. As shown in (34), the error probability is conditioned on D i.i.d. random variables $\{\gamma_j'\}$. Hence, the unconditional error probability is given by

$$P_e(D)=\int_0^\infty\cdots\int_0^\infty P_e(D|\{\gamma_j'\})\prod_{j=1}^{D}\mathcal{P}_{\gamma_j'}(\gamma_j')d\gamma_1'\cdots d\gamma_D'\tag{36}$$

where $\mathcal{P}_{\gamma_j'}(\gamma_j')$ is the *induced* density [17] of γ_j'. Since modulation symbol duration, $T_s(q_j)$, is a function of γ_j', the

induced density is different from the fading density in (10) but is given by [17]

$$\mathcal{P}_{\gamma_j'}(\gamma_j') = \frac{f_{\gamma_j'}(\gamma_j')}{E_f} T_s(\gamma_j') \tag{37}$$

where $T_s(\gamma_j')$ is the modulation symbol duration, $f_{\gamma_j'}(\gamma_j')$ is given by (10) with γ_j' replaces γ and E_f is given by

$$E_f = \int_0^\infty \frac{f_{\gamma_j'}(\gamma_j')}{T_s(\gamma_j')}\, d\gamma_j'. \tag{38}$$

Because ξ_j depends on γ_j' in (34) and (35), standard method of considering $\sum_j \gamma_j'$ as a single random variable cannot be used. Direct evaluation of the above equation is virtually impossible. We have thus developed a simplified expression by decomposition of $P_e(D|\{\gamma_j'\})$ and this is explained in Appendix B. We just quote the results as follows:

$$P_e(D) = \frac{1}{2^{2ND-1}} \Bigg[K_0 g^D(0) + \sum_{k}^{ND-1} K_k \cdot \sum_{m=1}^{\min(k,D)} g^{D-m}(0) D(D-1)\cdots(D-m+1) \cdot \sum_{\vec{\mathbf{r}}_m} C_k(\vec{\mathbf{r}}_m) g(r_1)\cdots g(r_m) \Bigg] \tag{39}$$

where (dropping the index j because $\{\gamma_j'\}$ are i.i.d. and writing ξ_j as $\xi(\gamma')$), we have

$$\begin{aligned} g(r) &\stackrel{\text{def}}{=} \int_0^\infty [\xi(\gamma')\gamma']^r e^{-\xi(\gamma')\gamma'} \mathcal{P}_{\gamma'}(\gamma')\, d\gamma' \\ &= \int_{\zeta_0}^{\zeta_1} \left(\tfrac{1}{16}\gamma'\right)^r \exp\left(-\tfrac{1}{16}\gamma'\right) \mathcal{P}_{\gamma'}(\gamma')\, d\gamma' \\ &\quad + \int_{\zeta_1}^{\zeta_2} \left(\tfrac{1}{8}\gamma'\right)^r \exp\left(-\tfrac{1}{8}\gamma'\right) \mathcal{P}_{\gamma'}(\gamma')\, d\gamma' + \cdots \\ &\quad + \int_{\zeta_6}^{\zeta_7} (8\gamma')^r e^{-8\gamma'} \mathcal{P}_{\gamma'}(\gamma')\, d\gamma'. \end{aligned} \tag{40}$$

Hence, $g(r)$ is easy to evaluate numerically. The average normalized throughput of VRNOM, $\overline{\eta}$, in bits per basic symbol is given by

$$\overline{\eta} = \mathcal{E}[\eta] = \int_0^\infty \left[\frac{1}{\xi(\gamma')}\right] f_{\gamma'}(\gamma')\, d\gamma'. \tag{41}$$

Note that *induced* density in (37) is not used here since the basic symbol duration is a constant.

2) Combined Fast Fading and Shadowing: The analysis of P_e is essentially the same as the previous subsection. However, because shadowing is a slow process, many symbol durations are affected by the same amount despite the use of interleaving. Hence, the error probability $P_e(D)$ in (39) is actually conditioned on a single[11] random variable called the local mean, $\overline{\gamma}'$. This local mean is modeled as log-normal distribution as described in Section III-B and is distributed as (11) with $\overline{\gamma}'$ replaces $\overline{\gamma}$. The unconditioned error probability is given by

$$P_e(D) = \int_0^\infty P_e(D|\overline{\gamma}') f_{\overline{\gamma}'}(\overline{\gamma}')\, d\overline{\gamma}' \tag{42}$$

where $P_e(D|\overline{\gamma}')$ is calculated using (39) with the given $\overline{\gamma}'$. Note that the *induced* density for $\overline{\gamma}'$ reduces to the original *log-normal* distribution since modulation symbol duration is independent of $\overline{\gamma}'$. The average normalized throughput, $\overline{\eta}$, in bits per basic symbol of VRNOM is given by

$$\overline{\eta} = \mathcal{E}[\eta] = \mathcal{E}\left[\frac{1}{\xi(\gamma')}\right]$$

where expectation is taken over $f_{\overline{\gamma}'}(\overline{\gamma}')$ and $f_{\gamma'|\overline{\gamma}'}(\gamma'|\overline{\gamma}')$.

V. Simulations

Simulations are performed to verify the analytical bound derived and to investigate the VRNOM performance in some practical situations that are difficult to analyze. The multiple access channel is modeled as a two-user channel with the total interference modeled as Gaussian noise as in (23). Complex channel noise is generated by two independent streams of Gaussian samples. Correlated channel fading is generated by low pass filtering of white Gaussian samples. Channel state estimation and prediction are simulated using the model described in Section II. Shadowing is modeled as statistical variation of local mean, $\overline{\gamma}$ on top of the variation of γ. Since it is a slow process, we assume a *block interference* model [18] for simplicity. A long block of fading shares an identical local mean taken from a *log-normal* distribution (11). Independent local mean sample is used between different long blocks.

VI. Results and Discussions

The performance of the VRNOM scheme is compared with that of the reference fix-rate code.[12]

A. Rayleigh Fading Only

For *constant BER* operation, the BER and the average normalized throughput, $\overline{\eta}$, against average reference SIR, $\overline{\gamma}$, are shown in Fig. 5(a) and (b) with different values of control parameter, ζ_1, at $N = 1$. The analytical BER bound and the analytical throughput obtained are close to the simulation results especially at high SIR. From Fig. 5(a), the BER curves of the VRNOM scheme flatten (we call it *plateau*) when $\overline{\gamma}$ reaches the adaptation range, achieving the *constant BER* purpose. This is because the switching thresholds of the VRNOM scheme makes the instantaneous BER relatively insensitive to the variation of instantaneous SIR(γ) in the adaptation range. Different ζ_1 gives different adaptation range and different BER level at the plateau. Note that along the BER curve of the reference code, we always have a normalized throughput of 1. However, along the BER curves of the VRNOM scheme, the normalized throughput, $\overline{\eta}$, varies as $\overline{\gamma}$.

[11] Note that it is incorrect to replace $\mathcal{P}_{\gamma'}(\gamma')$ by $\int \mathcal{P}_{\gamma'|\overline{\gamma}'}(\gamma') f_{\overline{\gamma}'}(\overline{\gamma}')\, d\overline{\gamma}'$ in (36) because this implies that we have independent shadowings between successive symbols.

[12] The chosen reference fix-rate code is close to optimal within the class of constraint-length 4 codes in Rayleigh fading with noncoherent detection. Hence, the comparison is fair.

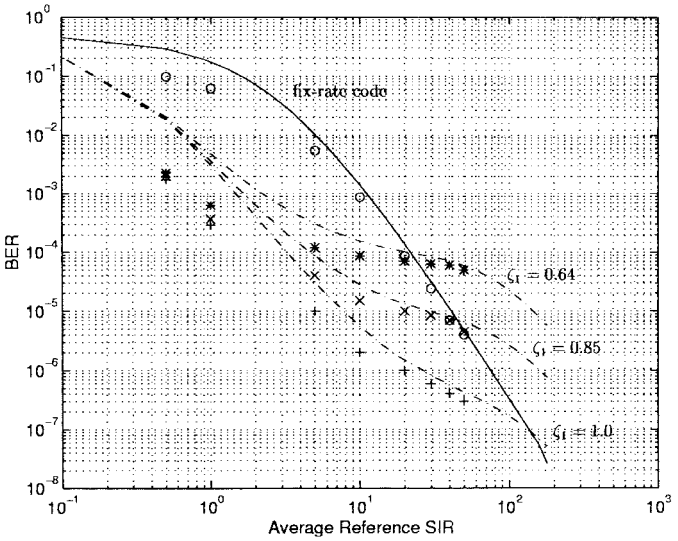

(a)

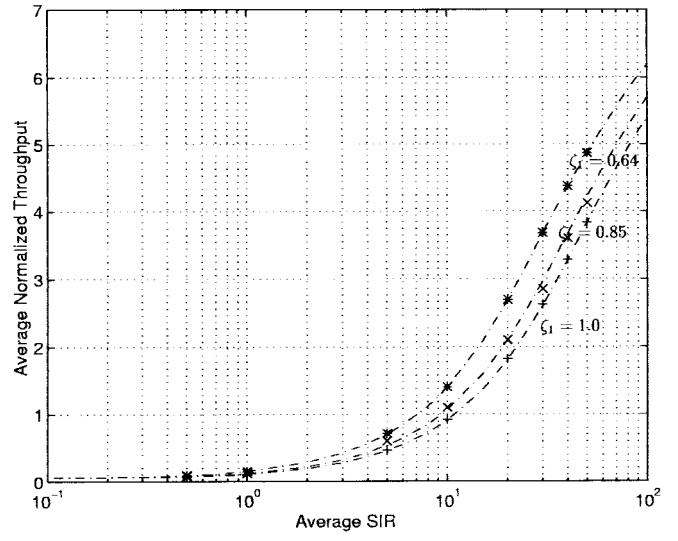

(b)

Fig. 5. Comparisons of BER and throughput performances for fix-rate reference code (solid line) and VRNOM scheme (dotted lines) in Rayleigh fading channel with $N = 1$. "×," "○," "∗," and "+" denote simulation results (varying throughputs along BER curves of VRNOM schemes).

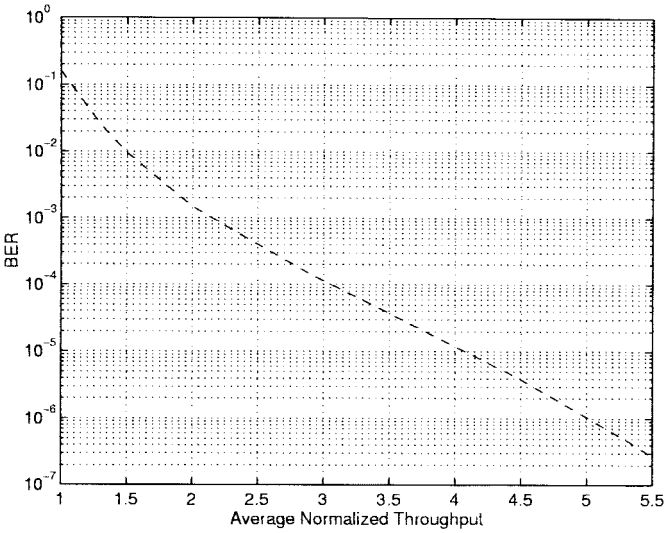

(a)

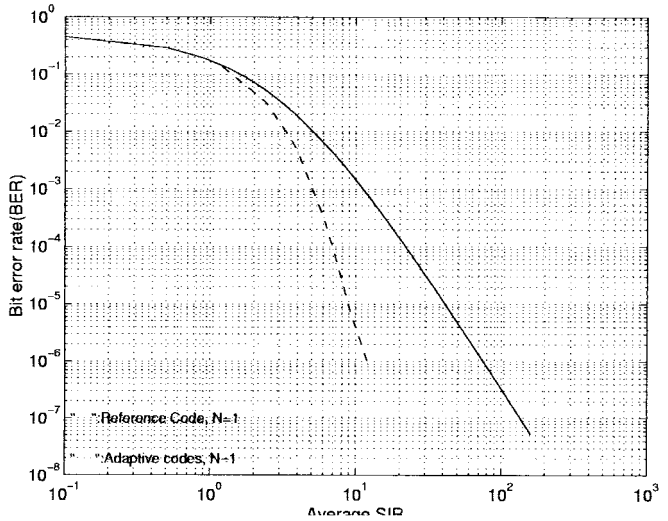

(b)

Fig. 6. Performances comparisons of VRNOM scheme and fix-rate code in Rayleigh fading channel with $N = 1$.

At high SIR, we trade a higher throughput with lower than necessary BER. On the other hand, at low SIR, the BER is kept low at the expense of lower throughput. The variation of throughput for VRNOM scheme is shown in Fig. 5(b).

Because of the variable throughput along the BER curves, to have a meaningful comparison, we should compare the relative throughput gain based on the same BER and the same average SIR. The relative throughput gain against the BER is shown in Fig. 6(a) for $N = 1$. For example, at BER = 10_{-2}, 10^{-4}, and 10^{-6}, the throughput gains relative to the fix-rate reference code are 1.5, 3, and 5, respectively. On the other hand, for *constant throughput* operation, the normalized throughput of VRNOM is kept constant at one and hence, comparison with the reference code can be made directly by considering the SIR gain. This is shown in Fig. 6(b) for $N = 1$. For example, at BER = 10^{-2}, 10^{-4}, and 10^{-6}, the SIR gains are 2, 5, and 8 dBm, respectively. Hence, VRNOM gives a significant improvement in both the SIR and the average throughput when frequency diversity is not effective. This is the case in some microcellular and indoor propagation channels where the coherent bandwidth can reach up to 10 MHz.

Fig. 7 shows the SIR gains for the VRNOM at $N = 3$. At $N = 3$, the SIR gains at BER = 10^{-2}, 10^{-4}, and 10^{-6} are 1.1, 2, and 3.1 dB. Hence, as the diversity branch in RAKE receiver increases, the performance gains of the VRNOM scheme drop. This is because the increased frequency diversity suppresses signal variation due to Rayleigh fading and hence, VRNOM scheme cannot benefit as much as the case without diversity.

B. Combined Rayleigh Fading, Shadowing, and Power Control

For *constant BER* operation, the BER of VRNOM scheme and fix-rate reference code in combined Rayleigh fading and shadowing channel are plotted against the average SIR ($\mu_{\overline{\gamma}}$) in Fig. 8. The shadowing process is slow and successive

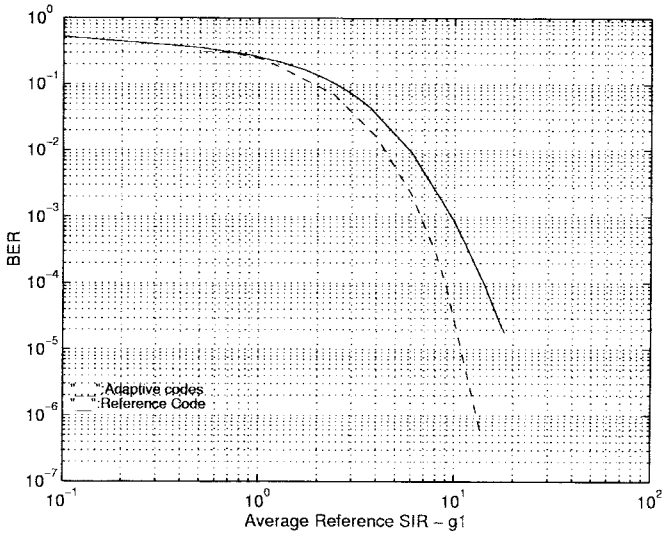

Fig. 7. Performance comparisons of VRNOM scheme and fix-rate code in Rayleigh fading channel with $N = 3$.

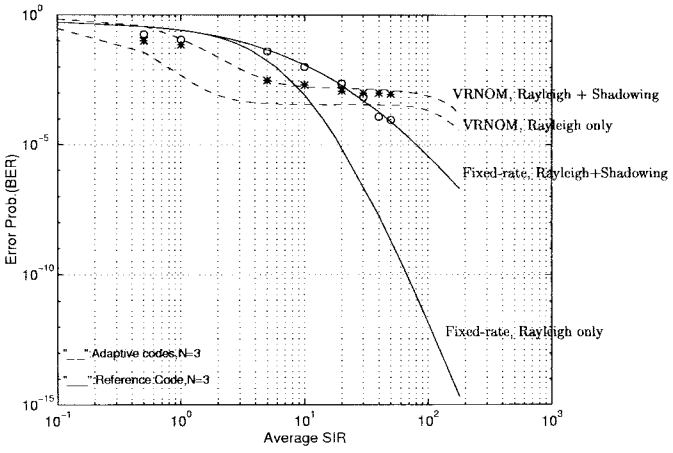

Fig. 8. Performance of VRNOM in channel with combined Rayleigh fading and shadowing, $N = 3$ (varying throughputs along BER curves of VRNOM).

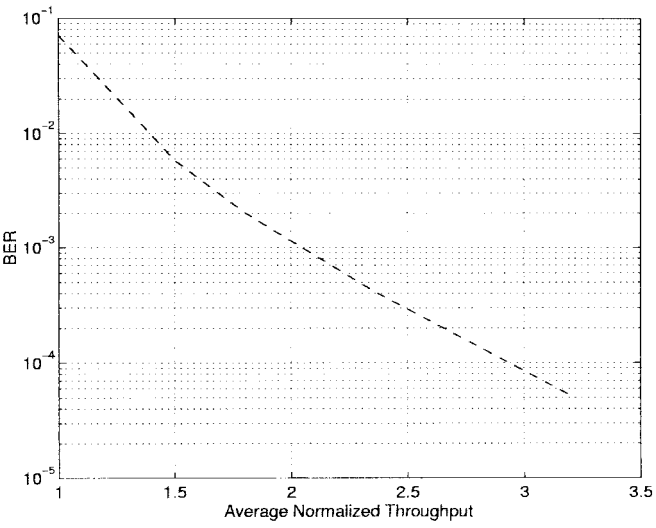

(a)

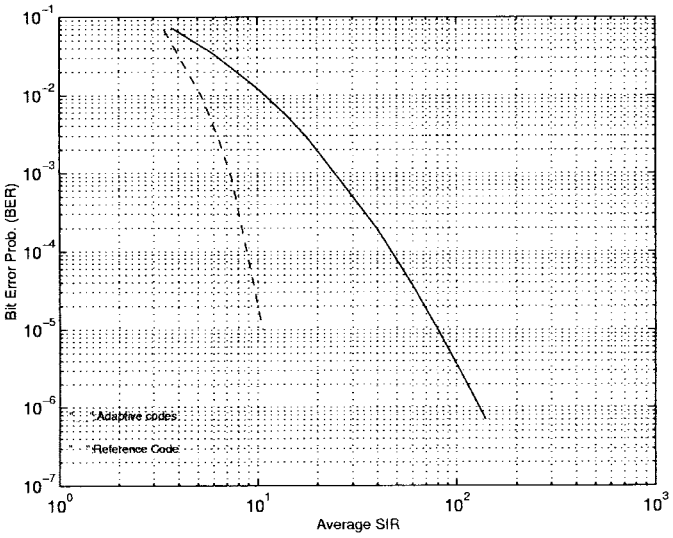

(b)

Fig. 9. Performance comparisons of VRNOM scheme and fix-rate code in channel with combined Rayleigh fading and shadowing, $N = 3$.

symbols are affected by the same amount despite the use of interleaver. Furthermore, microdiversity by the RAKE receiver is not effective in combating shadowing. Hence, in Fig. 8, the BER of the fix-rate reference code degrades severely under shadowing.

However, VRNOM scheme is relatively robust against shadowing. This is because of the plateau effect in the BER curves of VRNOM. The BER is less sensitive to the variations of $\overline{\gamma}$ in the adaptation range. This is illustrated in Fig. 8 where the degradation of BER for VRNOM scheme is small when $\mu\overline{\gamma}$ is between 6–20 dB. Outside this adaptation range, the BER is degraded in the same way as the reference code.

Similar to Section VI-A, the relative throughput gain against BER with shadowing is plotted in Fig. 9(a). The relative throughput gains at BER = 10^{-2} and 10^{-4} are 1.3 and 2.8, respectively. On the other hand, the SIR gain under *constant throughput* operation in shadowing channel is plotted in Fig. 9(b). The corresponding SIR gains with shadowing are 3.8 and 7 dB, respectively. Hence, VRNOM scheme is effective in combating shadowing.

C. Effect of Finite Interleaving—Assumption (i)

The effect of finite interleaving depth on VRNOM performance is investigated by simulation. We assume $f_dT_s = 10^{-2}$ which corresponds to 75 km/h at 40 k reference symbols/s. Fig. 10 shows the results of 100 $\times$ 1000, 100 $\times$ 300, and 2 $\times$ 2 interleaving depth. for the Rayleigh fading channel with $N = 1$. $\zeta_1 = 0.54$ is used for the VRNOM scheme. Both the VRNOM scheme and the fix-rate reference code suffer degradations due to the correlated fading. However, in all circumstances, the VRNOM scheme always out-performs the fix-rate code. For example, at $\overline{\gamma} = 5.5$ where the VRNOM scheme have an average throughput of 1, the SIR gains of the VRNOM scheme are 5.6 and 10.7 dB in the situations of 100 $\times$ 300 and 2 $\times$ 2 interleaving depths. The gains are even greater than the case of ideal interleaving. This is because fix-rate code degrades more than the VRNOM with finite interleaving depth. Therefore, VRNOM scheme are shown to be useful even in a very slow fading situation.

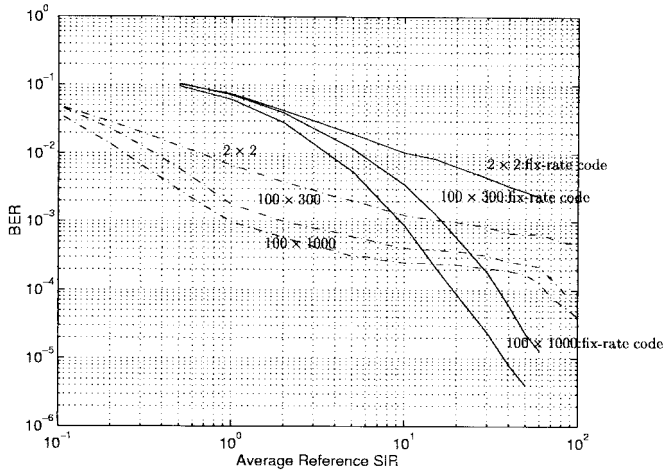

Fig. 10. Effects of finite interleaving. Mobile speed is equal to 75 km/h and reference symbol rate is 40k reference symbols/s.

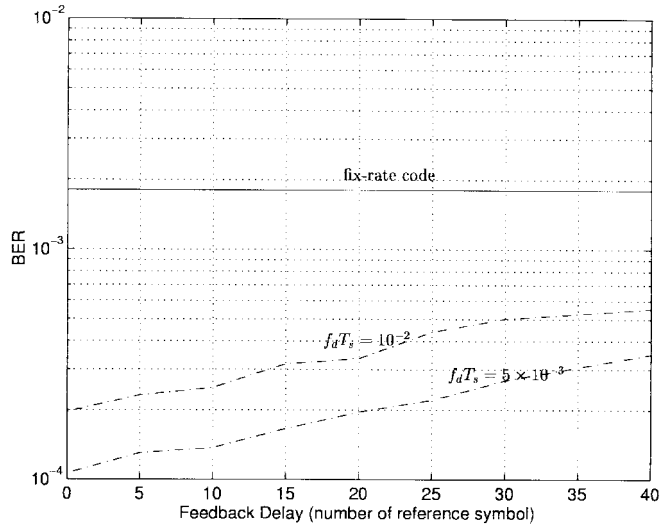

Fig. 11. Effect of feedback delay and practical channel state prediction. $P_f = 50$, $P_2 = 17$, $\overline{\gamma} = 8$, and $\overline{\eta} = 1$.

D. Effect of Nonideal Channel Prediction and Feedback Delay—Assumption (ii)

We assume the feedback period, $P_f = 50$, with a prediction filter order, $P_2 = 17$. The BER of the VRNOM scheme against Δ at $f_dT_s = 5 \times 10^{-3}$ and 10^{-2} are shown in Fig. 11. The degradation increases as the fading rate increases. At moderate feedback delays such as $\Delta = 20$ reference symbols, the BER's of VRNOM at $f_dT_s = 5 \times 10^{-3}$ and 10^{-2} are 10 and 3 times smaller than that of fix-rate code respectively. Hence, VRNOM is robust to feedback delay.

E. Effect of Mobile Speed

The BER against average SIR of VRNOM at $f_dT_s = 5 \times 10^{-3}$, $f_dT_s = 10^{-2}$, and $f_dT_s = 3 \times 10^{-2}$ are plotted in Fig. 12 with $N = 1$, $\Delta = 0$. The degradation in BER at higher fading rate is due to less accurate channel state prediction at the transmitter.

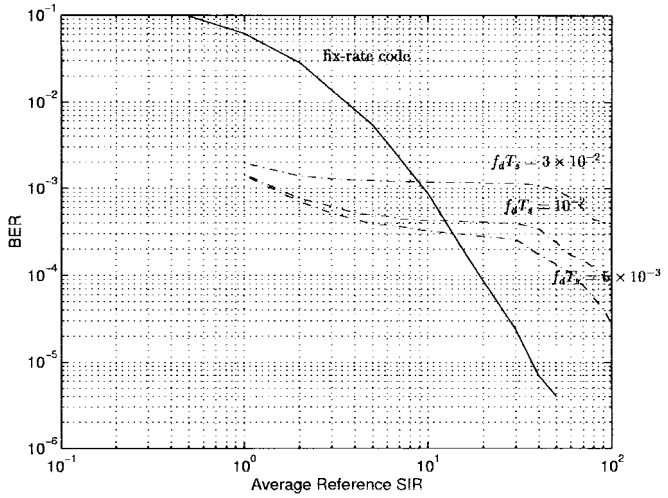

Fig. 12. Effect of mobile speed on VRNOM $N = 1$, $\Delta = 0$.

VII. Conclusion

In this paper, we propose a variable rate adaptive coding scheme (VRNOM) that uses *constant input* VRACE design in DS-CDMA systems. Performance is compared with a reference fix-rate code. Analytical bound is derived to evaluate the BER of VRNOM scheme under ideal situations. Simulations are done to verify the numeric results and to study the effects of finite interleaving depth, channel state estimation and prediction error, feedback delay, and mobile speed. Results obtained from theory matched the simulation results closely. Two cases, namely channel with Rayleigh fading only and channel with combined Rayleigh fading and shadowing, are considered.

VRNOM scheme is found to be very effective in combating Rayleigh fading with little frequency diversity. However, the improvement decreases gradually as the degree of frequency diversity increases. This is because frequency diversity suppresses large signal fluctuation in Rayleigh fading channel and hence the VRNOM scheme becomes less superior than the fix-rate code.

Fix-rate coding and microdiversity are not effective in combating shadowing because successive symbols are affected by the same amount despite interleaving. However, the VRNOM scheme is found to be relatively robust under shadowing.

Furthermore, the VRNOM scheme always out-performs the fix-rate code even when finite interleaving depth, finite feedback delay, estimation, and prediction errors in channel state and fading rate are taken into account.

References

[1] S. M. Alamouti and S. Kallel, "Adaptive trellis-coded multiple-phase-shift keying for Rayleigh fading channels," *IEEE Trans. Commun.*, vol. 42, pp. 2305–2314, June 1994.

[2] B. Vucetic, "An adaptive coding scheme for time-varying channels," *IEEE Trans. Commun.*, vol. 39, pp. 653–663, May 1991.

[3] J. K. Cavers, "Variable-rate transmission for Rayleigh fading channels," *IEEE Trans. Commun.*, vol. 20, pp. 15–22, Feb. 1972.

[4] H. Matsuoka, S. Sampei, and N. Morinaga, "Adaptive modulation system with punctured convolutional code for high quality personal communication systems," in *Proc. IEEE ICUPC'95*, Nov. 1995, pp. 22–26.

[5] T. Ue, S. Sampei, and N. Morinaga, "Symbol rate and modulation level controlled adaptive modulation/TDMA/TDD for personal communication systems," in *Proc. IEEE VTC'95*, July 1995, pp. 306–310.
[6] W. T. Webb and R. Steele, "Variable rate QAM for mobile radio," *IEEE Trans. Commun.*, vol. 43, pp. 2223–2230, July 1995.
[7] M. D. Yocoub, *Foundations of Mobile Radio Engineering*, 2nd ed. New York: McGraw-Hill, 1986.
[8] L. M. A. Jalloul and J. M. Holtzman, "Performance analysis of DS-CDMA with noncoherent M-ary orthogonal modulation in multipath fading channels," *IEEE J. Select. Areas Commun.*, vol. 12, pp. 862–870, June 1994.
[9] C. Kchao and G. L. Stuber, "Analysis of a direct-sequence spread-spectrum cellular radio system," *IEEE Trans. Commun.*, vol. 41, pp. 1507–1516, Oct. 1993.
[10] J. G. Proakis, *Digital Communications*, 2nd ed. New York: McGraw-Hill, 1989.
[11] A. J. Viterbi, "The orthogonal-random waveform dichotomy for digital mobile personal communication," *IEEE Personal Commun. Mag.*, vol. 42, pp. 18–24, Mar. 1994.
[12] G. L. Turin, "Introduction to spread-spectrum antimultipath techniques and their application to urban digital radio," *Proc. IEEE*, vol. 68, pp. 328–353, Mar. 1980.
[13] E. Geraniotis and M. B. Pursley, "Performance of coherent direct-sequence spread-spectrum communications over specular multipath fading channels," *IEEE Trans. Commun.*, vol. 33, pp. 502–508, June 1985.
[14] ———, "Performance of noncoherent direct-sequence spread-spectrum communications over specular multipath fading channels," *IEEE Trans. Commun.*, vol. 34, pp. 219–226, Mar. 1986.
[15] M. B. Pursley, "Performance evaluation for phase-coded SSMA communications—Part I: System analysis," *IEEE Trans. Commun.*, vol. 8, pp. 795–799, Aug. 1977.
[16] N. L. Johnson, *Continuous Univariate Distributions*, 2nd ed. New York: Houghton Mifflin, 1970, vol. 2.
[17] K. N. Lau and S. V. Maric, "Variable rate adaptive channel coding for coherent and noncoherent Rayleigh fading channel," in *Proc. IEEE ICPWC'97*, Bombay, India, Dec. 1997.
[18] R. J. Mceliece and W. E. Stark, "Channels with block interference," *IEEE Trans. Inform. Theory*, vol. 30, pp. 44–53, 1984.
[19] S. J. Mason, "Feedback theory-further properties of signal-flow graphs," *Proc. IRE*, July 1956, vol. 44, pp. 920–926.
[20] K. N. Lau, "Variable rate adaptive channel coding for mobile wireless systems," Ph.D. dissertation, Univ. of Cambridge, Cambridge, U.K. Also, [Online]. Available HTTP: http://www.eee.hku.hk/~knlau

Vincent K. N. Lau received the B.Eng. degree (1st Honors with Distinction) from the University of Hong Kong, Pokulam, Hong Kong, 1992, and the Ph.D. degree from the University of Cambridge in mobile communications in 1997.

He joined the Hong Kong Telecom after graduation as a Project Engineer, where he later became a Systems Engineer. He obtained the Sir Edward Youde Memorial Fellowship and the Croucher Foundation in 1995. In 1997, he joined Lucent Technologies-Wireless Core Technology as a member of the technical staff. He is currently engaged in the third generation wide-band CDMA development. In 1999, he is now an Assistant Professor at the University of Hong Kong. His research interests include information theory, adaptive channel coding and modulation, power control, and CREST factor control algorithms.

Svetislav V. Maric graduated from the University of Novi Sad and the University of Rochester and received the B.S., M.S., and Ph.D. degrees in 1986, 1987, and 1990, respectively.

He was the Assistant Professor at the City College of New York from 1991 to 1995. He was with the University of Cambridge from 1995 to 1997. Since then, he has joined Qualcomm as a Senior Engineer and is currently working on the call processing for IS-41, IS-95 cellular, and globalstar system. His research interests include frequency hopping code design, resource allocation, and queuing theory.